DOI: 10.1002/adma.201601075
Article type: Communication

Small Molecule / Polymer Blend Organic Transistors with Hole Mobility Exceeding 13 cm^2/Vs

*Alexandra F. Paterson, Neil D. Treat, Weimin Zhang, Zhuping Fei, Gwenhivir Wyatt-Moon, Hendrik Faber, George Vourlias, Panos A. Patsalas, Olga Solomeshch, Nir Tessler, Martin Heeney, Thomas D. Anthopoulos**

[*] A. F. Paterson, G. Wyatt-Moon, H. Faber, Prof. T. D. Anthopoulos
Department of Physics and Centre for Plastic Electronics,
Imperial College London,
South Kensington, London SW7 2AZ (UK)
E-mail: t.anthopoulos@ic.ac.uk

Dr. Neil D. Treat
Department of Materials, Imperial College London,
South Kensington, SW7 2AZ (UK)

Prof. Weimin Zhang,
College of Chemistry and Chemical Engineering Guangxi,
University for Nationalities, Nanning 530006, P. R. China

Dr. Zhuping Fei, Prof. M. Heeney
Department of Chemistry and Centre for Plastic Electronics,
Imperial College London,
South Kensington, London SW7 2AZ (UK)

Prof. George Vourlias, Prof. P. A. Patsalas
Department of Physics, Laboratory of Applied Physics,
Aristotle University of Thessaloniki
GR-54124 Thessaloniki, Greece

Dr. O. Solomeshch, Prof. N. Tessler
Sara and Moshe Zisapel Nano-Electronic Center,
Department of Electrical Engineering,
Technion - Israel Institute of Technology,
Haifa 3200, Israel

Keywords: Organic thin-film transistor, small molecule polymer blends, organic semiconducting blends, solvent blend, phase separation

Solution-processed, organic electronics have received remarkable attention over the past two decades due to the exclusive capabilities that they offer in comparison to mainstream inorganic semiconductor technologies.[1] [2] The desire for roll-to-roll printed, transparent, flexible electronics with greater economic viability has driven extensive research in the field, leading to substantial advances in the electronic properties of organic materials. These developments are illustrated by the overall rise in charge carrier mobilities – a crucial figure of merit – in organic thin-film transistors (OTFTs).[1] [3] [4] Over the past few years, this evolution has not only allowed organics to outperform dominant inorganic technologies such as amorphous silicon (a-Si), but it has excelled to the point that solution-processed organic transistors have now surpassed the benchmark mobility of 10 cm^2/Vs, moving OTFTs into the realm of industrial applications.[5] [6] [7] [8] [9] [10] [11] [12]

Organic semiconducting blends consisting of a small molecule and a polymer – renowned for their complexity as well as their advantageous electronic qualities – provide one of the most auspicious systems for realising the application of OTFTs in future electronic technologies. [4] [13] [14] Small molecules are well-known for their high charge carrier mobilities due to their high crystallinity, however they are difficult to process from a solution-phase.[15] [16] [17] Polymers, on the other hand, offer superior solution-processing qualities and produce uniform thin-films, but they are generally characterised by lower charge carrier mobility values.[17] [18] Blending small molecules with polymers has been shown to combine the high electrical performance traditionally associated with the small molecule with the superior film-forming attributes of the polymer, leading to semiconducting systems that combine the best of both worlds.[13] [14] [19] The 1st generation blend was introduced in 2009 by Hamilton *et al* when they blended the small-molecule 2,8-difluoro-5,11-bis(triethylsilylethynyl)anthradithiophene (diF-TES ADT) with the semiconducting polymer poly(triarylamine) (PTAA), resulting in OFETs with mobilities of 2.4 cm^2/Vs.[13] The excellent performance of the diF-TES

ADT:PTAA blend is attributed to the vertical phase separation of the two material components that results in a layer of high mobility polycrystalline small-molecule on top of a layer of polymer that acts as a binder.[4] [14] [20] This unique microstructure has been shown to reduce the energetic disorder in the transistor channel through the formation of conductive grain boundaries [21] that appear to mediate charge transport between polycrystalline domains. [14] In 2012, the development of the 2nd generation blend by Smith *et al* further demonstrated that the choice of polymer binder in the blend is of critical importance, with factors such as electronic energy levels and intrinsic polymer charge carrier mobility values being conducive in attaining organic transistors with very high charge carrier mobilities (>5 cm^2/Vs).[14] However, one interesting question that still remains is whether the charge carrier mobility of the blend system can be further increased to levels comparable to state-of-the-art OTFTs.[5] [7] [9] [11] [12] Such an advancement would impact the field of printed electronics by enabling the realisation of inexpensive, high-performance organic microelectronics that can be manufactured using scalable processing techniques.

Here, we report the development of 3rd generation hole-transporting organic blend semiconductors and their application in high mobility OTFTs. The small-molecule 2,7-dioctyl[1]benzothieno[3,2-b][1]benzothiophene (C_8-BTBT) [**Figure 1(a)**] was chosen due to its high solubility in various organic solvents as well as its ability to form large intermolecular overlaps arising from well-ordered molecular arrays, which under certain circumstances can lead to exceptionally high hole mobilities.[5] [7] [22] As the complementary polymer binder we selected the indacenodithiophene-benzothiadiazole (C_{16}IDT-BT) [**Figure 1(a)**] primarily due to its good solubility, high hole mobility (3.6 cm^2/Vs)[23] [24] [25] and comparable highest occupied molecular orbital (HOMO) energy level to that of the C_8-BTBT [**Figure 1(b)**].[26] [27] Using this unique combination of materials we have demonstrated solution-processed OTFTs with hole mobility values in excess of 13 cm^2/Vs. Key to our success is the incorporation of a

third molecular component, namely $C_{60}F_{48}$[28] [29] which acts as both a *p*-dopant and an electron scavenger. The use of solvent mixtures for dissolving the C_8-BTBT and C_{16}IDT-BT was also investigated and has been shown to have a remarkable influence on the resulting layer morphology and overall transistor performance.

Top-gate bottom-contacts transistors [**Figure 1(c)**] with channel lengths (L) in the range of 30-100 µm and a fixed channel width (W) of 1 mm, were fabricated using the C_8-BTBT:C_{16}IDT-BT (1:4 wt. ratio) blend deposited from a chlorobenzene (CB) solution (for details see *Experimental Section*). Although a range of C_8-BTBT:C_{16}IDT-BT compositional ratios were investigated, devices based on 1:4 wt. ratio yield the highest performance for this particular set of materials employed further details of which will be discussed later. **Figure 1(d)** shows a representative set of transfer characteristics measured at two different drain voltages (V_D). As-prepared OTFTs exhibit ambipolar transport behaviour with a prominent *p*-channel character as well as high operating voltages and significant hysteresis. Although the former property is attributed to the use of a thick Cytop layer (~900 nm) and its low dielectric constant (~2.1), the origin of the hysteresis is unknown and is most likely attributed to significant energetic disorder in the blend. Despite these nonidealities, the blend OTFTs exhibit an improved maximum hole mobility value of ~4.7 cm^2/Vs, compared to control devices made of C_8-BTBT (~2.6 cm^2/Vs) and C_{16}IDT-BT (~3.1 cm^2/Vs). This is a key observation that demonstrates the potential of this particular blend, indicating that blending C_{16}IDT-BT with C_8-BTBT results in passivation of grain-boundaries and improved hole-transport between C_8-BTBT rich regions, in an analogous manner to the 1st and 2nd generation blend systems discussed earlier.[13],[14] The subsequent inferior OTFT operating characteristics will not be considered in detail here, however, we believe that the performance improves with lower ratios of small-molecule to polymer as this encourages miscibility between the two materials leading to an improved layer microstructure.

There are a few potential reasons for the large operating hysteresis and high threshold voltages (V_{TH}) observed in C_8-BTBT:C_{16}IDT-BT transistors. One possibility is the existence of high energetic disorder due to the presence of deep trap states similar to those found in the 1st generation blends.[20] This energetic disorder may partially originate from the difference in the HOMO energies of C_8-BTBT and C_{16}IDT-BT (~100 meV) [**Figure 1(b)**] and/or from the presence of microstructural defects;[20] the presence of chemical impurities and the polymer molecular weight distribution may also play a role.[30] Due to this energetic disorder, high gate fields are required to fill the hole traps and eventually switch-on the channel current. However, once the transistor enters saturation, it is able to sustain large channel currents which is indicative of the blend's high hole mobility.

To examine whether energetic disorder is indeed responsible for the observed operating hysteresis, we have attempted to *p*-dope the C_8-BTBT:C_{16}IDT-BT blend by introducing a molecular dopant. In such ternary blend systems the dopant molecules are expected to accept electrons from the semiconducting materials leaving behind positively charged holes. This doping process can lead to the deactivation of hole traps that may contribute to the non-ideal transport characteristics seen in **Figure 1(d)**. To this end, recent work has shown that – under certain circumstances – doping organic semiconductors can indeed yield OTFTs and integrated circuits with improved operating characteristics.[31] [32] To assess the impact of doping, different molecular dopants were investigated with the most promising being the fluorinated fullerene derivative $C_{60}F_{48}$ [**Figure 2(a)**].[33] [34] [35] The attractive properties associated with $C_{60}F_{48}$ include a large molecular size that is expected to reduce its diffusivity in the solid state and a characteristically large electron affinity [**Figure 2(b)**]; because of these unique attributes, $C_{60}F_{48}$ has been used successfully as *p*-dopant for numerous carbon-based materials.[29] [36] [37] [38]

Figure 2(c) shows representative measured transfer characteristics for a *p*-doped C_8-BTBT:C_{16}IDT-BT:$C_{60}F_{48}$(1%) OTFT processed from CB. We investigated a range of dopant molar weight (wt.) percentages (0.01%, 0.1%, 1%, 5% and 10%) and found that the addition of 1% $C_{60}F_{48}$ in the C_8-BTBT:C_{16}IDT-BT blend has a profound impact on the transistors' operating characteristics. Specifically, we observe a dramatic reduction in both the operating hysteresis and V_{TH} of the device, both indicative of moderate *p*-doping. Increasing the $C_{60}F_{48}$ to 5% and 10% results in large off-currents and reduced on/off ratios due to an increase in hole concentration. Additionally, electron transport is fully supressed due to the presence of $C_{60}F_{48}$ molecules that act as deep electron traps. The most important effect, however, is the significant improvement in the hole field-effect mobility which now reaches values up to 7.8 cm^2/Vs, with an average value of 5.3 cm^2/Vs calculated from 10 transistors fabricated on the same substrate. These are amongst the highest hole mobilities reported to date for both solution processed C_8-BTBT and C_{16}IDT-BT based transistors and clearly highlight the technological potential of this particular doped blend system.

In addition to *p*-doping, we have also explored the use of alternative solvents as a means of improving the morphology and hence the long-range charge transport in the C_8-BTBT:C_{16}IDT-BT:$C_{60}F_{48}$(1%) blend. The choice of solvent is known to have a significant influence on film formation and has been exploited extensively for crystal engineering[39] [40] [41] as the solvent can impact the microstructure by effecting the thermodynamics of the solution, crystallisation kinetics and also the interface structure of the formed crystals.[40] For these reasons, a variety of solvents and solvent-blends have been explored previously in organic electronics as a simple manufacturing approach to morphological and hence electrical performance optimisation.[15] [19] [42] [43] [44] [45] [46] **Figure 2(d)** shows the transfer characteristics of a C_8-BTBT:C_{16}IDT-BT:$C_{60}F_{48}$(1%) blend OTFT processed from the higher boiling point

(207 °C) solvent 1,2,3,4-tetrahydronaphthalene (tetralin). Although the devices exhibit hysteresis-free and low V_{TH} operation, the hole transport is significantly hindered when compared to devices processed from CB, with the hole mobility values ranging between 0.1 and 1.6 cm^2/Vs.

We were able to significantly improve the performance and device-to-device parameter distribution of the C_8-BTBT:C_{16}IDT-BT:$C_{60}F_{48}$ blend OTFTs by using a solvent mixture composed of tetralin and CB (tetralin:CB). As with the single solvent formulations, we investigated both the impact of dopant concentration as well as the C_8-BTBT loading ratio. **Figure S2** shows the evolution of the work function (WF), obtained via Kelvin probe measurements, and HOMO energy level, evaluated via atmospheric photoemission spectroscopy, in the C_8-BTBT:C_{16}IDT-BT blend as a function of $C_{60}F_{48}$ concentration. In this plot 0% molar wt. represents the energy levels of pristine C_8-BTBT:C_{16}IDT-BT. Close examination of the data reveals that incorporation of 1% molar wt. $C_{60}F_{48}$ leads to a drastic shift in the WF by approximately -0.5 eV. The HOMO energy on the other hand remains unchanged as would be expected. Increasing the $C_{60}F_{48}$ concentartion to 5% molar wt. reduces the WF further by ~0.2 eV to -4.9 eV. These measurements provide direct evidence of *p*-doping of C_8-BTBT:C_{16}IDT-BT by $C_{60}F_{48}$.

In **Figure 3(a)** we show a representative set of transfer characteristics measured for a top-gate, bottom-contact C_8-BTBT:C_{16}IDT-BT:$C_{60}F_{48}$(1%) OTFT processed from tetralin:CB. As with the previous solvent formulations, 1:1 volume ratio of C_8-BTBT:C_{16}IDT-BT combined with 1% $C_{60}F_{48}$ was found to yield best performing transistors (**Figure S3**). The maximum hole mobility calculated in saturation from these devices was in excess of 13 cm^2/Vs, with an average value of 9.4 cm^2/Vs taken over 16 devices. In **Figure 3(b)** we summarise the calculated hole mobilities with the associated spreads and mean values obtained from C_8-BTBT:C_{16}IDT-

BT:$C_{60}F_{48}$(1%) OTFTs processed from the three different solvent solutions. The use of tetralin:CB as the solvent not only increases the hole mobility of the transistors compared to the OTFTs processed from CB or tetralin, but also improves other device operating characteristics such as the channel current on-off ratio ($I_{ON/OFF} > 10^3$) and device-to-device parameter spread [**Figure 3(b)**]. On the basis of these results we conclude that the addition of $C_{60}F_{48}$ (1%) as a *p*-dopant combined with a tetralin:CB solvent blend results in OTFTs with significantly improved performance characteristics.

To investigate the significant differences in device performance, we studied the morphology of the various blend layers using polarized optical microscopy (POM), atomic force microscopy (AFM) and scanning electron microscopy (SEM). In **Figures 4(a-c)** we show the POM images of C_8-BTBT:C_{16}IDT-BT:$C_{60}F_{48}$(1%) blend films processed from tetralin:CB, CB and tetralin, where solvent-dependant morphologies are observed. This is not surprising, as the solvent is known to play an important role on the crystallisation and phase separation of the different components.[4] [39] [47] [19] For example, films deposited from tetralin:CB [**Figure 4(a)**] are characterised by long crystalline C_8-BTBT domains of random shapes. Films fabricated from CB [**Figure 4(b)**], on the other hand, consist of more rounded, spherulite-like polycrystalline domains closely resembling those seen in semiconducting blends composed of 2,8-difluoro-5,11-bis(triethylsilylethynyl)anthradithiophene (diF-TESADT) and poly(triarylamine) (PTAA).[13] Finally, films spin-cast from tetralin appear highly discontinuous with high surface roughness [**Figure 4(c)**]. Scanning electron microscopy (SEM) imaging [**Figure S4**] provides key clues on why the hole mobilities obtained from CB and tetralin formulations are not as high as in devices processed from the tetralin:CB blend. Specifically, the SEM images in **Figure S4** show that the surface topography of pristine [**Figure S4(a)**] and $C_{60}F_{48}$ (1%) doped [**Figure S4(b)**] blend films processed from tetralin:CB appear continuous and very similar. On the contrary, layers processed from CB contain

cracks/perforations [**Figure S4(c)**] most likely due to residual-solvent effects[48] while tetralin layers exhibit strong phase separation. In the latter case, these non-ideal morphological features are believed to be the reasons for the lower mobilities measured for OTFTs processed from CB and tetralin solutions [**Figure 3(b)**].

The stark differences in the surface topography of the three layers are better illustrated in the high-resolution AFM images in **Figures 4(d-f)** and in the statistical distributions of surface heights and associated root mean square (RMS) surface roughness displayed in **Figure 4(g)**. Close examination of **Figure 4(g)** reveals that blend films processed from tetralin:CB exhibit significantly smoother surface topographies -manifested as narrow distribution of heights and lower RMS values- when compared to films processed from CB and tetralin where clear bi/multi-modal distributions (indicative of the presence of plateaus and valleys) are evident. The prominent bimodal surface topography seen in layers processed from tetralin is thought to be due to the high tetralin boiling point (207 °C) which allows C_8-BTBT to diffuse, crystallise and phase separate from the higher viscosity polymer, forming the polycrystalline domains seen in **Figure 4(f)** and in the SEM image of **Figure S4(d)**. In contrast, the surface of doped blend films processed from the lower boiling point CB (131°C) is characterised by what appears to be a continuous polycrystalline layer of C_8-BTBT.

The improved microstructure seen in layers of C_8-BTBT:C_{16}IDT-BT:$C_{60}F_{48}$(1%) processed from tetralin:CB and CB is further supported by the observation of molecular terracing. In **Figures 4(h)** we show a representative AFM line scan obtained from the highlighted region in **Figure 4(d)**, clearly indicating the formation of molecular terraces with step heights of 2.65 (±0.2) nm; this observation closely resembles the molecular terracing previously reported for high mobility C_8-BTBT layers/devices.[7] [22] [49] Similar molecular terracing features are also seen in layers processed from CB, but the terraces appear to be 2-3

molecules thick [~5.69 (±0.2) nm, **Figure 4(i)**] as opposed to the single molecular steps seen in blends processed from tetralin:CB [**Figure 4(h)**]. In contrast, no evidence of molecular terracing is observed in layers processed from the tetralin solutions where strong phase-separation between the two components is observed [see **Figure 4(f)** and **Figure S4(d)**].

It has been previously shown that C_8-BTBT layered crystallinity – which is known to form herringbone structures with lattice constants a = 0.593, b = 0.788 and c = 2.92 – favours hole transport along the film planes (x-y plane).[7] [50] It is therefore important to investigate the crystal structure and quality of the polycrystalline planes parallel to the C_8-BTBT:C_{16}IDT-BT:$C_{60}F_{48}$(1%) film surface, *i.e.* the charge carrier direction. To achieve this we have used an in-plane wide-angle x-ray diffraction (WAXD) technique. Both pristine and doped films of the C_8-BTBT:C_{16}IDT-BT blend processed from all three of the solvents were found to be crystalline with the main peaks associated mostly with the C_8-BTBT, as shown in **Figure 5(a)** and in more detail in **Figure S1**. Quantitative variations of the C_8-BTBT lamellar stacking dimensions (*i.e.* in-plane crystallite size) and the corresponding *d*-spacing between them do exist amongst the different samples. These variations were quantified by a Lorentzian peak fit analysis of the WAXD data and in particular the (003) planes of C_8-BTBT by Scherrer's and Bragg's formulae, respectively.[50] The corresponding results are summarised in the histogram in **Figure 5(b)**. It is evident that use of tetralin:CB as the solvent results in C_8-BTBT:C_{16}IDT-BT films with improved crystallinity and longer spatial separation between their lattice planes. These results suggest that the improved electrical performance of the *p*-doped C_8-BTBT:C_{16}IDT-BT:$C_{60}F_{48}$(1%) OTFTs might be the result of complementary effects from improved crystallinity along the z-direction (more well-defined phase separation) – which is supported by the WAXD data – and improved integrity and coherency in the x-y plane, as determined by AFM [**Figures 4(d-f)**] and SEM [**Figure S4**]. We note, however, that the observed structural differences along the growth direction (z-direction) are less prominent

compared to the morphology variations observed in the x-y planes detected by the AFM measurements, and therefore we might safely assume that the longer range continuity of the blend films in the x-y plane is the dominant factor for the enhanced electrical performance observed.

Finally, the vertical phase separation of the different materials in the best-performing C_8-BTBT:C_{16}IDT-BT:$C_{60}F_{48}$(1%) blend processed from tetralin:CB was studied using time-of-flight secondary ion mass spectrometry (ToF-SIMS). The Poisson corrected ion signals corresponding to the three molecular components are plotted in **Figure 5(c)** as a function of sputter time (with the air interface at x = 0 s). As the beam sputters through the depth of the film, the signals corresponding to C_8-BTBT and C_{16}IDT-BT decrease and increase respectively as a function of sputtering time. The step-wise nature of this change in elemental composition suggests a pseudo-bilayer microstructure with the C_8-BTBT segregating on the surface of the film. This vertical phase separation correlates with previously reported blend systems[13] [14] [20] making the C_8-BTBT:C_{16}IDT-BT:$C_{60}F_{48}$(1%) ideal for use in top-gate OTFTs. Interestingly, we find that the signal corresponding to the $C_{60}F_{48}$ appears almost entirely within the C_{16}IDT-BT layer located closer to the bottom interface (blend/substrate). One plausible explanation is that $C_{60}F_{48}$ is more soluble in the C_{16}IDT-BT compared to C_8-BTBT, and/or the crystallisation of C_8-BTBT tends to expel $C_{60}F_{48}$ causing this vertical phase separation to occur. Additionally, a strong signal associated with $C_{60}F_{48}$ is found at the air interface; this is consistent with the expected phase separation of the F^- rich compound as its presence at the air interface would tend to reduce the total surface energy of the system. An alternative explanation would be the presence of physical gaps (perforations) in the crystalline layer of C_8-BTBT at the top of the film which allow the sputtering beam to access the buried C_{16}IDT-BT:$C_{60}F_{48}$(1%) layer even at sputter time x = 0 s, leading to the apparent observation of ions associated with the two compounds being present at the surface in higher than expected concentrations.

A further implication of this unusual vertical material distribution is the unconventional nature of the doping mechanism that might be at work. By studying the energy band diagram in **Figure 2(b)** one may expect C_8-BTBT to *p*-dope more easily due to its higher ionization potential (-5.04 eV) as compared to C_{16}IDT-BT (-5.15 eV). However, since the dopant is distributed primarily within the polymer, it is reasonable to assume that free holes are generated within C_{16}IDT-BT and/or close to the mixed C_8-BTBT:C_{16}IDT-BT:$C_{60}F_{48}$(1%) interface region [**Figure 5(c)**]. Mobile excess holes can then contribute to the channel current via different processes including: (i) mediation of hole transport between the high mobility crystalline domains of C_8-BTBT due to the enhanced conductivity of C_{16}IDT-BT in a process similar to that observed in 1st generation blend OTFTs[21]; (ii) deactivation of hole traps present in the pristine blend OTFTs; (iii) transfer of holes to the polycrystalline top C_8-BTBT layer in a process similar to modulation doping of inorganic heterointerfaces. Although it is currently difficult to identify, with high degree of certainty, the dominant mechanism(s) responsible for the dramatic enhancement of the hole mobility observed, obtained results indicate the co-existence of more than one processes with most dominant the deactivation of hole traps.

In summary, we have developed solution-processed blend OTFTs with maximum hole mobility values in excess of 13 cm^2/Vs. We have achieved this by blending the small-molecule C_8-BTBT with the conjugated polymer C_{16}IDT-BT. Although the performance of the resulting OTFTs is moderate and highly variable, the introduction of the molecular *p*-dopant $C_{60}F_{48}$ (1% mol) in combination with a suitable solvent blend, significantly improve the hole transport properties, leading to transistors with maximum hole mobilities exceeding 13 cm^2/Vs. By considering additional processing improvements, we believe that it is feasible for the C_8-BTBT:C_{16}IDT-BT:$C_{60}F_{48}$(1%) transistors to reach hole mobilities close to the maximum value of 31.3 cm^2/Vs reported for single crystal C_8-BTBT based devices.[7]

Experimental Section

Material Preparation and Device Fabrication: C_{16}IDT-BT was prepared using previously reported procedures [51], while C_8-BTBT was purchased from Aldrich and used as received. The number average molecular weight for C_{16}IDT-BT was 66.5 Kg/mol with a dispersity (Đ) of 2.42 as measured by GPC in chlorobenzene at 80 ˚C against polystyrene standards. The C_8-BTBT:C_{16}IDT-BT blend solutions were prepared at a concentration of 10 mg/ml and at a small-molecule to polymer ratio of 1:4. Three solutions were made: one in tetralin, another in CB and a third in a solution that was comprised of tetralin and CB at a ratio of 1:1. $C_{60}F_{48}$ was added to each solution at 1% molar weight. TG-BC devices were fabricated on glass substrates. The glass substrates were cleaned in a detergent solution (DECON 90), acetone and isopropanol. 40nm thick Au source and drain electrodes were evaporated under vacuum onto a 5nm Al adhesion layer, before being treated with a pentafluorothiophenol (PFBT) self-assembling monolayer (SAM). The SAM treatment required the substrate to be submerged in a 5 mmol/L PFBT in isopropanol solution for 5 minutes. The semiconducting blend films were deposited from a solution heated to 50°C and applied via spin coating in a nitrogen atmosphere. Following spin coating, the films were placed on a hotplate for 5 minutes at 120°C and allowed to cool to room temperature (~23 ^{o}C). The fluoropolymer CYTOP was deposited via spin-coating to produce a 900 nm thick dielectric layer, which was then annealed for an hour at 50°C. Thermal evaporation through a shadow mask was then used to deposit a 50 nm thick Al gate.

Atomic Force Microscopy: An Agilent 5500 scanning probe microscope operating in tapping mode was used to gather information on both topography and phase of the semiconductor films. In order to accurately replicate the real-system, each film that was measured had the dielectric layer (CYTOP) deposited onto and removed from the semiconductor layer. Statistical and image analysis was undertaken using Gwyddion 2.39.

Time-of-flight secondary ion mass spectrometry (ToF-SIMS): An IONTOF ToF-SIMS V with a base pressure of 10^{-10} torr was used to measure depth profiles with a 2.5kV Ar cluster (1000 atoms, ~1 nA) sputter beam rastered across a 300 x 300 μm square. Negative ions were collected from the central 200 x 200 μm of the sputter crater using a Bi_3^+ (~0.5 pA) beam. The molecular signals used to construct the depth profiles correspond to ionized forms of the C_8-BTBT and C_{16}IDT-BT, i.e. $C_{30}H_{40}S_2^-$ and CNS^- respectively. The elemental signals of F^- and Si^- were used to construct the depth profiles of the $C_{60}F_{48}$ and silicon substrate, respectively.

In-plane Wide Angle X-ray Diffraction (WAXD): The crystal structures of the films were studied by in-plane (Bragg-Brentano geometry) WAXD using the CuKa monochromated line (λ=0.154 nm) in a Rigaku Ultima+ diffractometer. The anode high voltage and the filament current were 40 kV and 30 mA, respectively.

Kelvin Probe and Air Photoemission Measurements: The work function (WF) and HOMO levels of the doped/undoped blends and constituent materials were determined via the Kelvin Probe (KP) and air photoemission (APS) technique, respectively, using a scanning Kelvin Probe system (KP Technology, SKP5050/APS02) and silver as the KP reference material. Photoemission measurements were performed by scanning the wavelength of incident light between 6.2 and 4.4 eV and monitoring the photocurrent response. The HOMO level was then extracted using Fowler analysis, by plotting the cube-root of the photocurrent signal and extrapolation to the zero baseline [1]. All measurements were carried out in ambient atmosphere at room temperature and approx. 25 % relative humidity.

Scanning Electron Microscopy: The surface morphology was investigated using a LEO Gemini 1525 Field Emission Scanning Electron Microscope (FESEM) with the operating voltage at 5 kV.

Supporting Information

Supporting Information is available from the Wiley Online Library or from the author.

Acknowledgements

T.D.A. and A.F.P acknowledge financial support from Cambridge Display Technology (Company Number 2672530). O.S. acknowledges the support of the Center for Absorption in Science of the Ministry of Immigrant Absorption under the framework of the KAMEA Program.

Received: ((will be filled in by the editorial staff))
Revised: ((will be filled in by the editorial staff))
Published online: ((will be filled in by the editorial staff))

[1] H. Sirringhaus, *Advanced materials* **2014**, *26*, 1319-1335.

[2] H. Dong, X. Fu, J. Liu, Z. Wang, W. Hu, *Advanced materials* **2013**, *25*, 6158-6182.

[3] J. G. Labram, Y.-H. Lin, T. D. Anthopoulos, *Small* **2015**, *11*, 5472-5482.

[4] J. Smith, R. Hamilton, I. McCulloch, N. Stingelin-Stutzmann, M. Heeney, D. D. C. Bradley, T. D. Anthopoulos, *Journal of Materials Chemistry* **2010**, *20*, 2562-2574.

[5] Y. B. Yuan, G. Giri, A. L. Ayzner, A. P. Zoombelt, S. C. B. Mannsfeld, J. H. Chen, D. Nordlund, M. F. Toney, J. S. Huang, Z. N. Bao, *Nat Commun* **2014**, *5*, 3005.

[6] G. Kim, S.-J. Kang, G. K. Dutta, Y.-K. Han, T. J. Shin, Y.-Y. Noh, C. Yang, *J Am Chem Soc* **2014**, *136*, 9477-9483.

[7] H. Minemawari, T. Yamada, H. Matsui, J. Tsutsumi, S. Haas, R. Chiba, R. Kumai, T. Hasegawa, *Nature* **2011**, *475*, 364-367.

[8] Y. Diao, B. C. K. Tee, G. Giri, J. Xu, D. H. Kim, H. A. Becerril, R. M. Stoltenberg, T. H. Lee, G. Xue, S. C. B. Mannsfeld, Z. Bao, *Nat. Mater.* **2013**, *12*, 665-671.

[9] H. R. Tseng, H. Phan, C. Luo, M. Wang, L. A. Perez, S. N. Patel, L. Ying, E. J. Kramer, T. Q. Nguyen, G. C. Bazan, A. J. Heeger, *Advanced Materials* **2014**, *26*, 2993-2998.

[10] S. Kwon, J. Kim, G. Kim, K. Yu, Y.-R. Jo, B.-J. Kim, J. Kim, H. Kang, B. Park, K. Lee, *Advanced materials* **2015**, DOI:10.1002/adma.201502980.

[11] H. Iino, T. Usui, J.-i. Hanna, *Nat Commun* **2015**, *6*, 6828

[12] B. H. Lee, G. C. Bazan, A. J. Heeger, *Advanced materials* **2016**, *28*, 57-62.

[13] R. Hamilton, J. Smith, S. Ogier, M. Heeney, J. E. Anthony, I. McCulloch, J. Veres, D. D. C. Bradley, T. D. Anthopoulos, *Advanced Materials* **2009**, *21*, 1166-1171.

[14] J. Smith, W. M. Zhang, R. Sougrat, K. Zhao, R. P. Li, D. K. Cha, A. Amassian, M. Heeney, I. McCulloch, T. D. Anthopoulos, *Advanced materials* **2012**, *24*, 2441-2446.

[15] D. K. Hwang, C. Fuentes-Hernandez, J. D. Berrigan, Y. Fang, J. Kim, W. J. Potscavage, Jr., H. Cheun, K. H. Sandhage, B. Kippelen, *Journal of Materials Chemistry* **2012**, *22*, 5531-5537.

[16] D. Guo, T. Miyadera, S. Ikeda, T. Shimada, K. Saiki, *J Appl Phys* **2007**, *102*, 023706.

[17] C. D. Dimitrakopoulos, P. R. L. Malenfant, *Advanced materials* **2002**, *14*, 99-117.

[18] I. McCulloch, M. Heeney, C. Bailey, K. Genevicius, I. MacDonald, M. Shkunov, D. Sparrowe, S. Tierney, R. Wagner, W. Zhang, M. L. Chabinyc, R. J. Kline, M. D. McGehee, M. F. Toney, *Nat Mater* **2006**, *5*, 328-333.

[19] M. R. Niazi, R. Li, E. Qiang Li, A. R. Kirmani, M. Abdelsamie, Q. Wang, W. Pan, M. M. Payne, J. E. Anthony, D.-M. Smilgies, S. T. Thoroddsen, E. P. Giannelis, A. Amassian, *Nat Commun* **2015**, *6*, 8598.

[20] J. Smith, R. Hamilton, Y. Qi, A. Kahn, D. D. C. Bradley, M. Heeney, I. McCulloch, T. D. Anthopoulos, *Adv Funct Mater* **2010**, *20*, 2330-2337.

[21] S. Hunter, T. D. Anthopoulos, *Advanced materials* **2013**, *25*, 4320-4326.

[22] T. Izawa, E. Miyazaki, K. Takimiya, *Advanced materials* **2008**, *20*, 3388-3392.

[23] H. Bronstein, D. S. Leem, R. Hamilton, P. Woebkenberg, S. King, W. M. Zhang, R. S. Ashraf, M. Heeney, T. D. Anthopoulos, J. de Mello, I. McCulloch, *Macromolecules* **2011**, *44*, 6649-6652.

[24] I. McCulloch, R. S. Ashraf, L. Biniek, H. Bronstein, C. Combe, J. E. Donaghey, D. I. James, C. B. Nielsen, B. C. Schroeder, W. M. Zhang, *Accounts Chem Res* **2012**, *45*, 714-722.

[25] X. Zhang, H. Bronstein, A. J. Kronemeijer, J. Smith, Y. Kim, R. J. Kline, L. J. Richter, T. D. Anthopoulos, H. Sirringhaus, K. Song, M. Heeney, W. Zhang, I. McCulloch, D. M. DeLongchamp, *Nat Commun* **2013**, *4*, 2238.

[26] H. Kobayashi, N. Kobayashi, S. Hosoi, N. Koshitani, D. Murakami, R. Shirasawa, Y. Kudo, D. Hobara, Y. Tokita, M. Itabashi, *The Journal of Chemical Physics* **2013**, *139*, 014707.

[27] J. Soeda, Y. Hirose, M. Yamagishi, A. Nakao, T. Uemura, K. Nakayama, M. Uno, Y. Nakazawa, K. Takimiya, J. Takeya, *Advanced materials* **2011**, *23*, 3309-3314.

[28] O. Solomeshch, Y. J. Yu, A. A. Goryunkov, L. N. Sidorov, R. F. Tuktarov, D. H. Choi, J.-I. Jin, N. Tessler, *Advanced materials* **2009**, *21*, 4456-4460.

[29] Y. Smets, C. B. Stark, F. Schmitt, M. T. Edmonds, S. Lach, C. A. Wright, D. P. Langley, K. J. Rietwyk, A. Schenk, A. Tadich, M. Wanke, C. Ziegler, L. Ley, C. I. Pakes, *Org. Electron.* **2013**, *14*, 169-174.

[30] H. Klauk, *Organic Electronics: Materials, Manufacturing, and Applications*, Wiley, 2006.

[31] S. Rossbauer, C. Müller, T. D. Anthopoulos, *Adv Funct Mater* **2014**, *24*, 7116-7124.

[32] T. D. Anthopoulos, *Unconventional chemical doping of organic semiconducting materials* **2013**, WO 2013098648 A1.

[33] N. Tessler, O. Solomeshch, *Derivatized fullerene-based dopants for organic semiconductors* **2013**, US 8431434 B2.

[34] A. A. Gakh, A. A. Tuinman, J. L. Adcock, R. A. Sachleben, R. N. Compton, *J Am Chem Soc* **1994**, *116*, 819-820.

[35] L. G. Bulusheva, A. V. Okotrub, O. V. Boltalina, *The Journal of Physical Chemistry A* **1999**, *103*, 9921-9924.

[36] M. T. Edmonds, M. Wanke, A. Tadich, H. M. Vulling, K. J. Rietwyk, P. L. Sharp, C. B. Stark, Y. Smets, A. Schenk, Q. H. Wu, L. Ley, C. I. Pakes, *J Chem Phys* **2012**, *136*, 124701.

[37] A. Tadich, M. T. Edmonds, L. Ley, F. Fromm, Y. Smets, Z. Mazej, J. Riley, C. I. Pakes, T. Seyller, M. Wanke, *Appl Phys Lett* **2013**, *102*, 241601.

[38] K. J. Rietwyk, M. Wanke, H. M. Vulling, M. T. Edmonds, P. L. Sharp, Y. Smets, Q. H. Wu, A. Tadich, S. Rubanov, P. J. Moriarty, L. Ley, C. I. Pakes, *Phys Rev B* **2011**, *84*, 035404.

[39] A. S. Myerson, *Handbook of Industrial Crystallization: Second Edition*, Butterworth-Heinemann, Boston, 2001.

[40] K. Byrappa, T. Ohachi, *Crystal Growth Technology*, Springer, New York, 2003.

[41] M. B. Patrick Augustijns, *Solvent Systems and Their Selection in Pharmaceutics and Biopharmaceutics*, Springer, New York, 2007.

[42] M. Lada, M. J. Starink, M. Carrasco, L. Chen, P. Miskiewicz, P. Brookes, M. Obarowska, D. C. Smith, *Journal of Materials Chemistry* **2011**, *21*, 11232-11238.

[43] J. J. Chang, C. Y. Chi, J. Zhang, J. S. Wu, *Advanced materials* **2013**, *25*, 6442-6447.

[44] X. Li, B. K. C. Kjellander, J. E. Anthony, C. W. M. Bastiaansen, D. J. Broer, G. H. Gelinck, *Adv Funct Mater* **2009**, *19*, 3610-3617.

[45] S. Han, X. Yu, W. Shi, X. Zhuang, J. Yu, *Organic Electronics* **2015**, *27*, 160-166.

[46] J. F. Chang, B. Q. Sun, D. W. Breiby, M. M. Nielsen, T. I. Solling, M. Giles, I. McCulloch, H. Sirringhaus, *Chem Mater* **2004**, *16*, 4772-4776.

[47] K. Sangwal, *Additives and Crystallization Processes: From Fundamentals to Applications*, Wiley & Sons, New Jersey, 2007.

[48] P. S. Jo, D. T. Duong, J. Park, R. Sinclair, A. Salleo, *Chem Mater* **2015**, *27*, 3979-3987.

[49] M. Dohr, O. Werzer, Q. Shen, I. Salzmann, C. Teichert, C. Ruzie, G. Schweicher, Y. H. Geerts, M. Sferrazza, R. Resel, *Chemphyschem* **2013**, *14*, 2554-2559.

[50] J. y. Tsutsumi, S. Matsuoka, S. Inoue, H. Minemawari, T. Yamada, T. Hasegawa, *Journal of Materials Chemistry C* **2015**, *3*, 1976-1981.

[51] W. Zhang, J. Smith, S. E. Watkins, R. Gysel, M. McGehee, A. Salleo, J. Kirkpatrick, S. Ashraf, T. Anthopoulos, M. Heeney, I. McCulloch, *J Am Chem Soc* **2010**, *132*, 11437-11439.

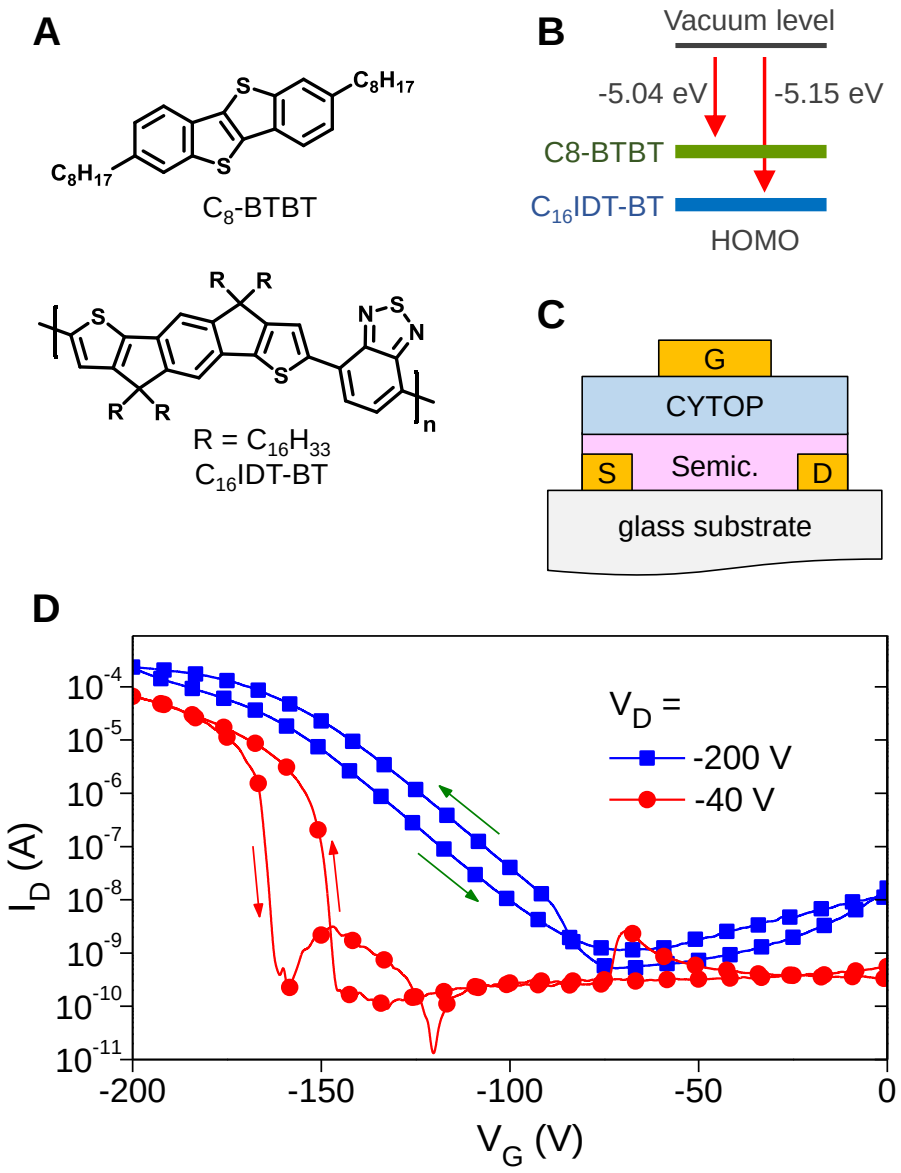

Figure 1. (a) Chemical structures of the small-molecule 2,7-dioctyl[1]benzothieno[3,2-b][1]benzothiophene (C_8-BTBT) and the indacenodithiophene-benzothiadiazole (C_{16}IDT-BT) polymer used in this work. (b) Highest occupied molecular orbital (HOMO) energy levels of C_8-BTBT and C_{16}IDT-BT measured via air photoemission. (c) Schematic of the top-gate, bottom-contact (TG-BC) transistor architecture used to study the charge transport properties of the various semiconducting materials. (d) Representative transfer characteristics measured for a C_8-BTBT:C_{16}IDT-BT blend-based transistor at V_D = -40 V and V_D = -200 V in nitrogen at room temperature.

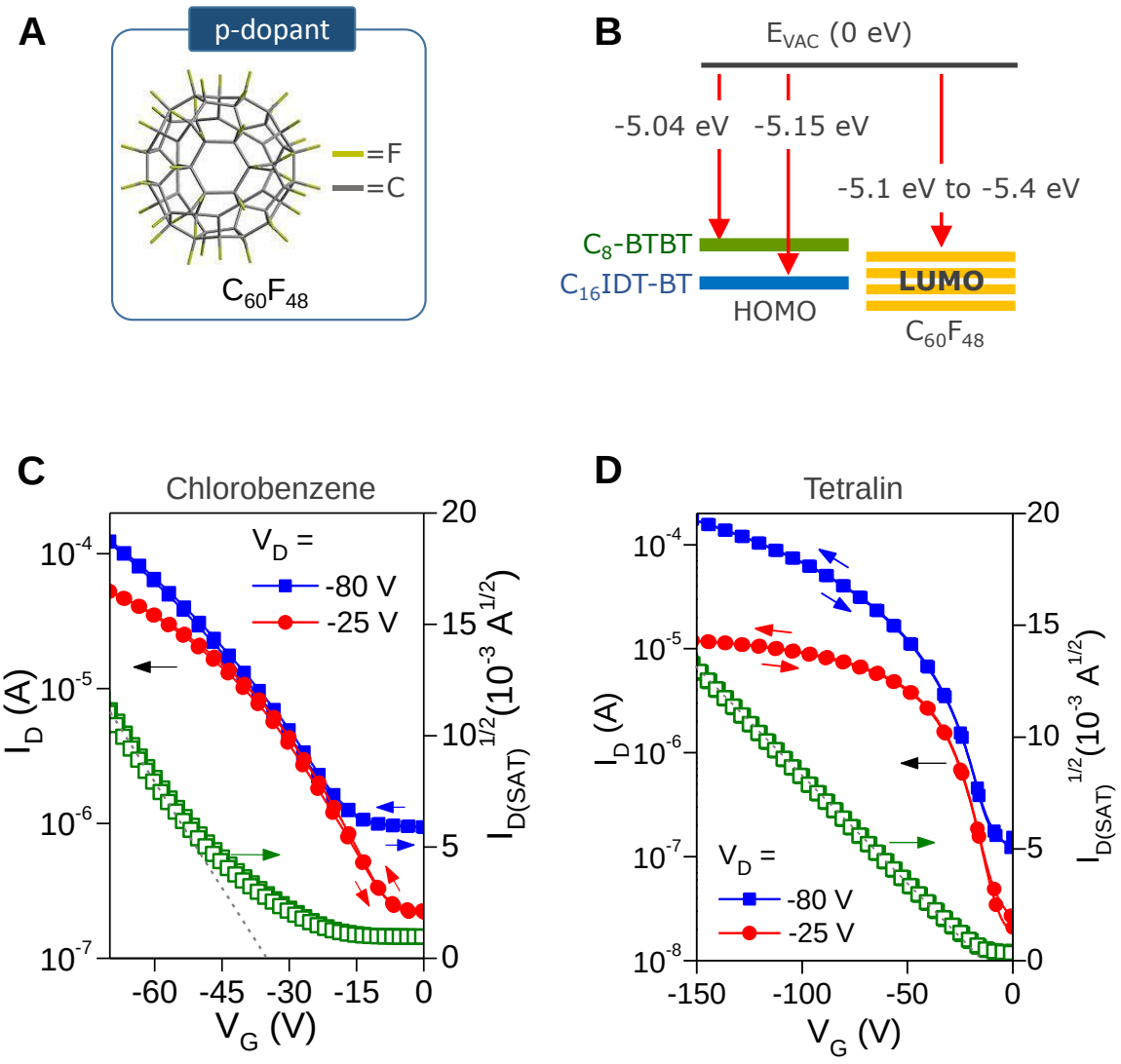

Figure 2. (a) Chemical structure of the molecular dopant $C_{60}F_{48}$. (b) HOMO energy levels of C_8-BTBT and C_{16}IDT-BT measured using air photoemission spectroscopy and the range of lowest unoccupied molecular orbital (LUMO) energies reported for $C_{60}F_{48}$.[29] [36] [37] [38] Representative transfer characteristics measured at V_D = -25 V and V_D = 80 V for two *p*-doped C_8-BTBT:C_{16}IDT-BT:$C_{60}F_{48}$(1%) blend transistors processed from chlorobenzene (c), and tetralin (d). Both transistors have channel length and width of 80 µm and 1000 µm respectively.

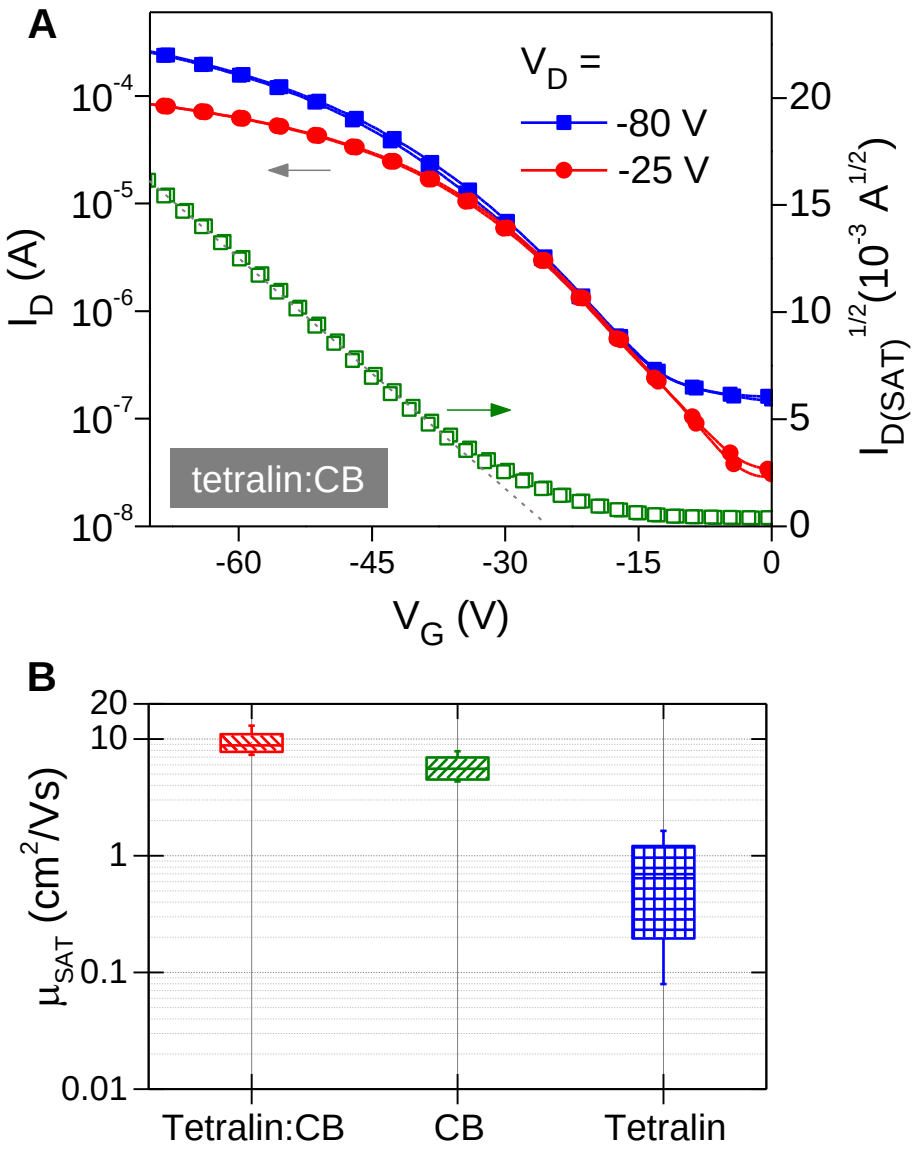

Figure 3. Representative transfer characteristics measured at V_D = -25 V and V_D = 80 V for a *p*-doped C_8-BTBT:C_{16}IDT-BT:$C_{60}F_{48}$(1%) blend transistor processed from 1:1 tetralin:CB solvent-blend; the transistor has channel length and width of 80 µm and 1000 µm respectively. (b) Box-and-whisker plot comparing the saturation mobilities measured for a number of transistors processed from tetralin:CB, chlorobenzene and tetralin solutions.

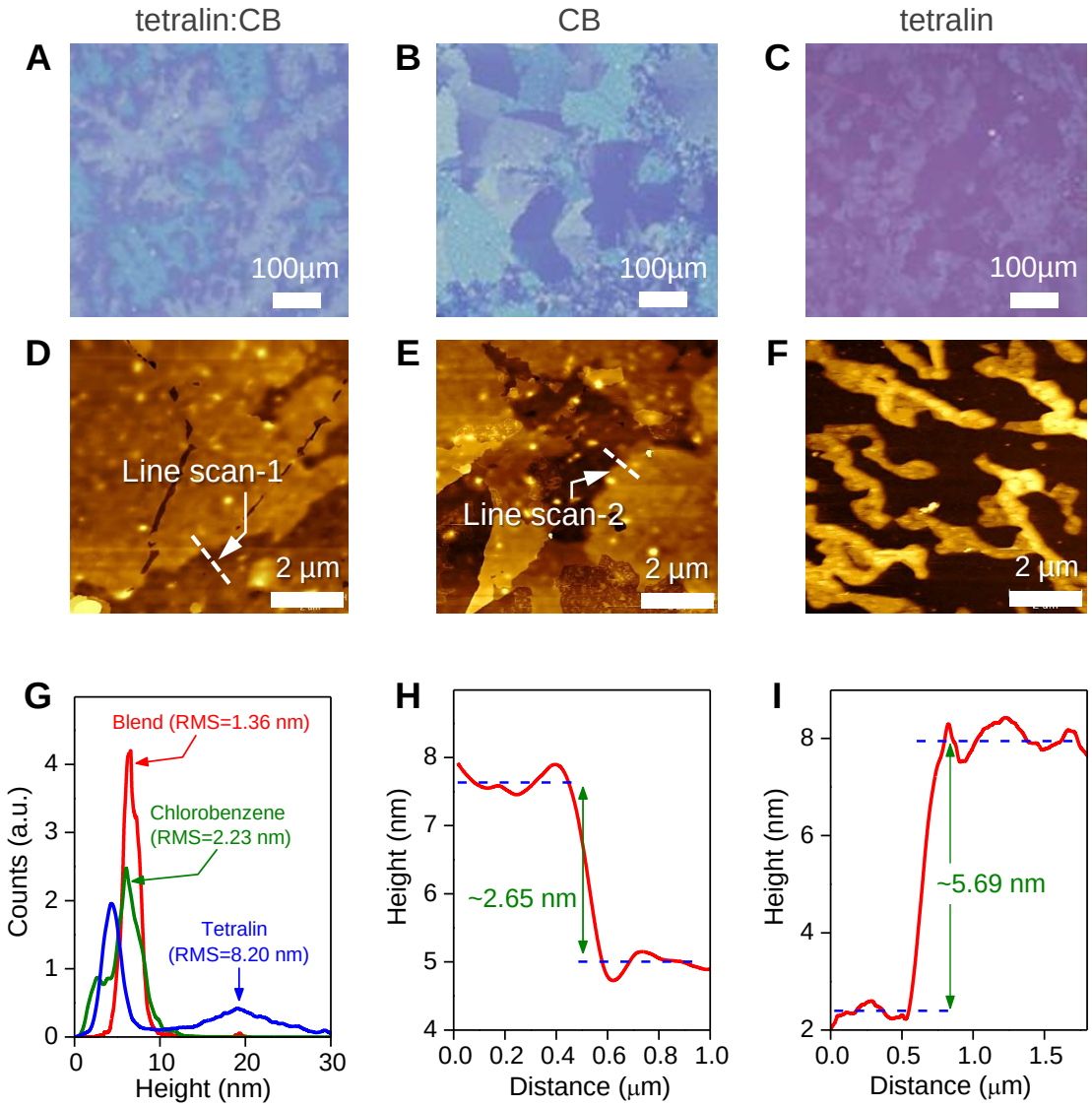

Figure 4. Polarized optical microscopy (POM) images of *p*-doped C_8-BTBT:C_{16}IDT-BT:$C_{60}F_{48}$(1%) blend films processed from (a) 1:1 tetralin:CB, (b) chlorobenzene and (c) tetralin solutions. (d-f) Atomic force microscopy (AFM) topography images of the same blend films shown in (a-c). (g) Surface height distribution histograms of the three films processed from the different solvent systems and corresponding root mean squared (r.m.s) surface roughness values. (h) Line-scan obtained from the highlighted area in the AFM image in (d) demonstrating molecular terracing of C_8-BTBT. (i) Line-scan obtained from the highlighted area of the AFM image in (e).

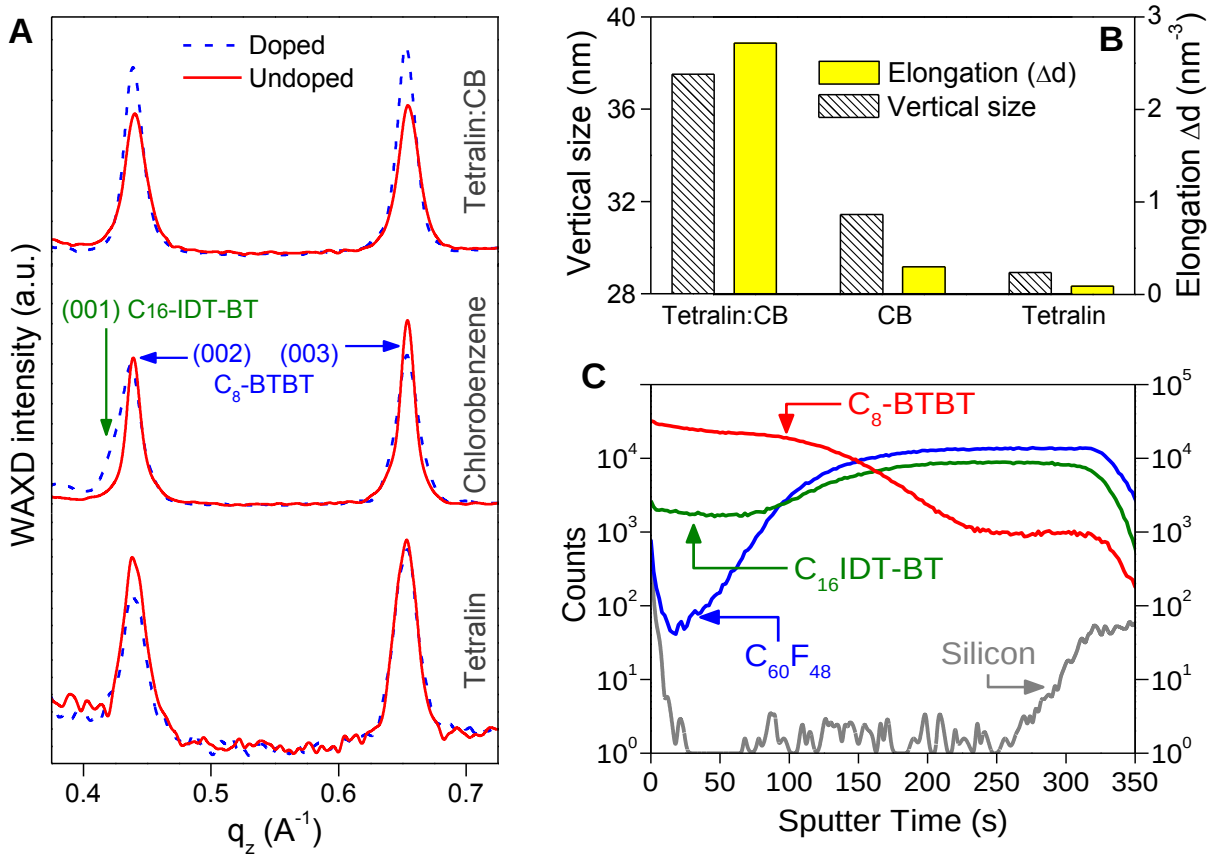

Figure 5. (a) Details of the in-plane WAXD measurements for the low index planes of the pristine and *p*-doped C_8-BTBT:C_{16}IDT-BT:$C_{60}F_{48}$(1%) films processed from tetralin:CB, chlorobenzene and tetralin. Solid and dashed lines stand for undoped and 1% $C_{60}F_{48}$ doped films respectively. (b) Shows the vertical (z-axis) crystallite size of C_8-BTBT for the three considered solvents, and the elongation of the (003) C_8-BTBT lattice plane spacing (Δd) for the pristine and *p*-doped blend films for the three considered solvents i.e. tetralin:CB, chlorobenzene and tetralin. (c) Time-of-flight secondary ion mass spectrometry (ToF-SIMS) data obtained for a representative *p*-doped C_8-BTBT:C_{16}IDT-BT:$C_{60}F_{48}$(1%) layer.

Table of Contents Entry

A ternary organic semiconducting blend based on the high hole mobility small-molecule C_8-BTBT, the polymer C_{16}ITD-BT and the molecular *p*-dopant $C_{60}F_{48}$, is developed and used in solution-processed organic transistors with maximum hole mobility in excess of 13 cm^2/Vs (**Figure**). We show that key to this development is the incorporation of the $C_{60}F_{48}$ dopant and the formation of a vertically phase-separated film microstructure.

Keyword: Organic thin-film transistor, small molecule polymer blends, organic semiconducting blends, solvent blend, phase separation

Alexandra F. Paterson, Neil D. Treat, Weimin Zhang, Zhuping Fei, Gwenhivir Wyatt-Moon, Hendrik Faber, George Vourlias, Panos A. Patsalas, Olga Solomeshch, Nir Tessler, Martin Heeney, Thomas D. Anthopoulos

Small Molecule / Polymer Blend Organic Transistors with Hole Mobility Exceeding 13 cm^2/Vs

ToC Figure

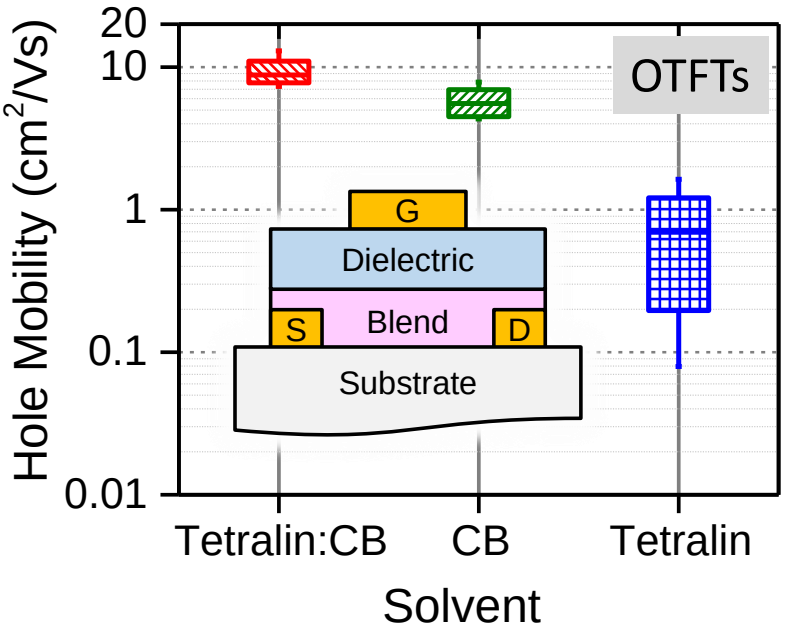

Supporting Information

Small Molecule / Polymer Blend Organic Transistors with Hole Mobility Exceeding 13 cm^2/Vs

*Alexandra F. Paterson, Neil D. Treat, Weimin Zhang, Zhuping Fei, Gwenhivir Wyatt-Moon, Hendrik Faber, George Vourlias, Panos A. Patsalas, Olga Solomeshch, Nir Tessler, Martin Heeney, Thomas D. Anthopoulos**

Section S1. Experimental Results

Samples of pristine C_8-BTBT and C_{16}IDT-BT were measured as references of the single constituents of the blends. All the C_{16}IDT-BT samples were found to be amorphous, independent of the solvent and diffraction geometry. Only a very broad peak around q_z=0.15 A^{-1} has been recorded and it is believed to correspond to alkyl chains [Ref S1] and it is consistent with the halo observed in corresponding GIWAXS data. The pure C_8-BTBT, on the other hand, was found to be highly crystalline; the observed in-plane WAXD peaks are consistent with the monoclinic structure of C_8-BTBT and its reported lattice sizes and geometrical characteristics [Ref S2], and therefore the corresponding Miller indices were firmly assigned (see **Figure S1**). The blends (both doped and undoped) were found to be crystalline with the main peaks being associated mostly with the C_8-BTBT (as shown in **Figure S1**) for representative samples. The main peaks observed in the in-plane WAXD are consistent with the GIWAXS data along the in-plane direction. In the case of the doped blend in a chlorobenzene solution, there are strong indications of partial crystallization of the C_{16}IDT-BT. In particular, there is a faint peak at q_z=0.9 A^{-1} (**Figure S1**, dashed line) that may correspond to the (002) C_{16}IDT-BT planes [Ref S3], as well as a fine structure of the peak around q_z=0.45 A^{-1}, which could only be explained by the emergence of the (001) C_{16}IDT-BT planes; this potentially indicates a stronger phase separation in this case, which is in strong agreement with the ToF-SIMS data.

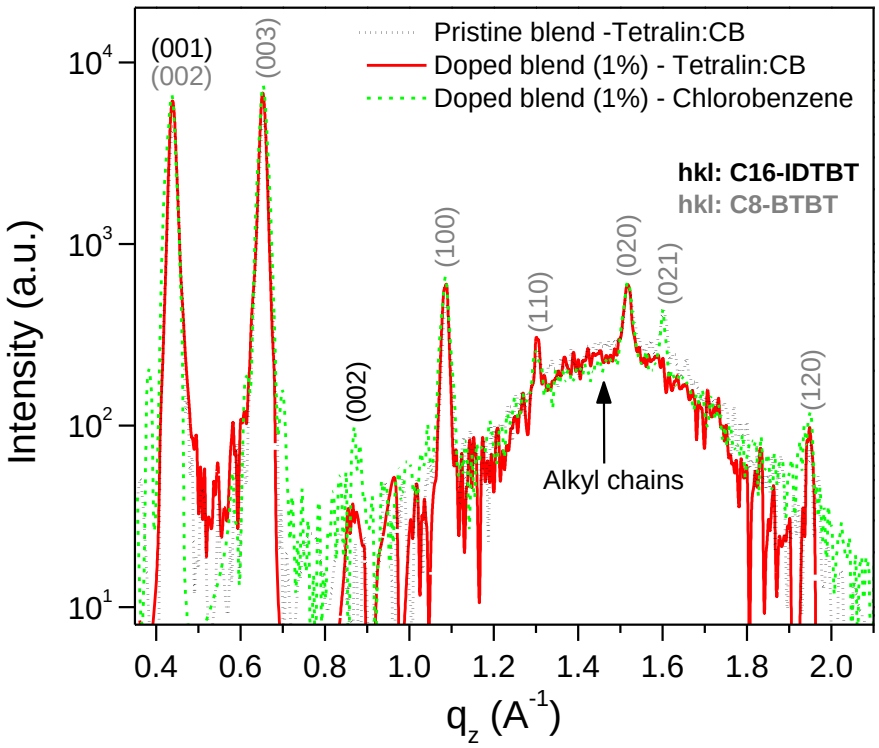

Figure S1. In-plane wide angle x-ray diffraction (WAXD) of selected samples showing the main diffraction peaks obtained for the pristine and $C_{60}F_{48}$(1%)-doped blend films processed from tetralin:CB and Chlorobenzene solvents.

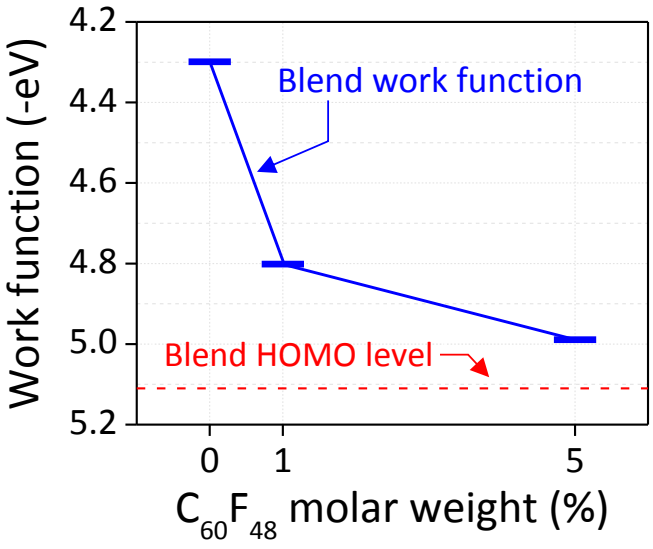

Figure S2. Kelvin Probe and air photoemission measurements were employed to calculate the work function (WF) and HOMO energy level of the C_8-BTBT:C_{16}IDT-BT blend as a function of $C_{60}F_{48}$ concentration (dopant) with 0 wt.% representing the energy levels for the pristine

(undoped) C_8-BTBT:C_{16}IDT-BT blend. As can be seen, WF shifts towards the HOMO energy level of the C_8-BTBT:C_{16}IDT-BT blend with the addition of $C_{60}F_{48}$ up to 5% molar wt.. This shift provides direct evidence of p-doping of C_8-BTBT:C_{16}IDT-BT by $C_{60}F_{48}$.

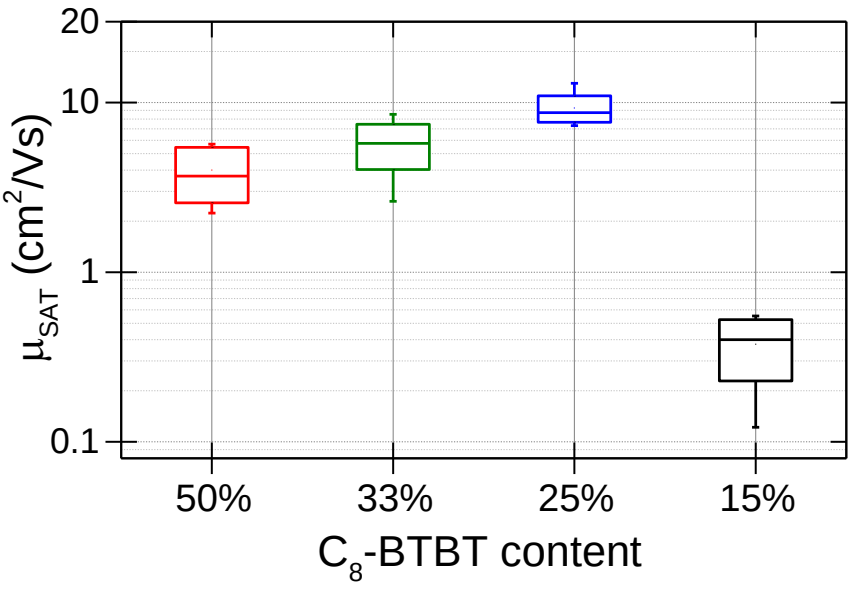

Figure S3. Box-and-whisker plot comparing the saturation mobilities (μ_{SAT}) measured for a number of transistors processed from C_8-BTBT:C_{16}IDT-BT:$C_{60}F_{48}$(1%) blends containing 50%, 33%, 25% and 15% C_8-BTBT. Transistors based on the 1:4 small-molecule:polymer blends were found to be the best performing.

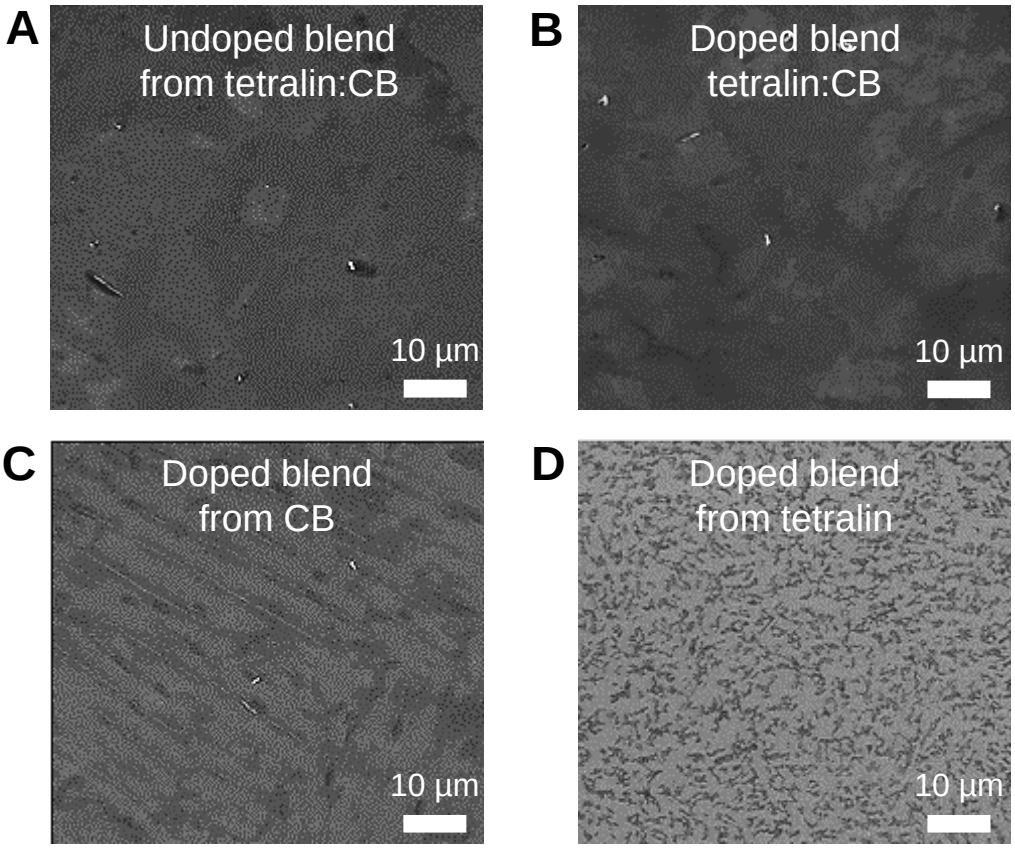

Figure S4. Scanning Electron Microscopy images of the various organic semiconducting blends investigated. (a) Shows a representative image of the pristine C_8-BTBT:C_{16}IDT-BT blend processed from 1:1 wt.% tetralin:CB, while (b) displays the SEM image of a *p*-doped C_8-BTBT:C_{16}IDT-BT:$C_{60}F_{48}$(1%) blend film processed from 1:1 tetralin:CB. Images (c) and (d) are for the same blend formulations but processed form chlorobenzene and tetralin solutions, respectively. The images of the doped and non-doped 1:1 tetralin:CB show very little difference in surface morphology.

SI References

[S1] 25th Anniversary Article: Organic Field-Effect Transistors: The Path Beyond Amorphous Silicon, H. Sirringhaus, Adv. Mater. **2014**, *26*, 1319–1335.

[S2] Molecular Ordering of High-Performance Soluble Molecular Semiconductors and Re-evaluation of Their Field-Effect Transistor Characteristics, T. Izawa, E. Miyazaki, K. Takimiya, Adv. Mater. **2008**, *20*, 3388–3392.

[S3] Molecular origin of high field-effect mobility in an indacenodithiophene–benzothiadiazole copolymer, X. Zhang, H. Bronstein, A.J. Kronemeijer, J. Smith, Y. Kim, R.J. Kline, L. J. Richter, T. D. Anthopoulos, H. Sirringhaus, K. Song, M. Heeney, W. Zhang, I. McCulloch, D. M. DeLongchamp, Nature Comm. **2013**, *4*, art. no.2238.